Boosting the resolution of low-field 15 N relaxation experiments on intrinsically disordered proteins with triple-resonance NMR

Zuzana Jaseňáková, Vojtěch Zapletal, Petr Padrta, Milan Zachrdla, Nicolas Bolik-Coulon, Thorsten Marquardsen, Jean-Max Tyburn, Lukáš Žídek, Fabien Ferrage, Pavel Kadeřávek

Boosting the resolution of low-field ^{15}N relaxation experiments on intrinsically disordered proteins with triple-resonance NMR

Zuzana Jaseňáková[†], Vojtěch Zapletal[†], Petr Padrta[†], Milan Zachrdla, Nicolas Bolik-Coulon, Thorsten Marquardsen, Jean-Max Tyburn, Lukáš Žídek, Fabien Ferrage*, Pavel Kadeřávek*

Zuzana Jaseňáková, Vojtěch Zapletal, Lukáš Žídek:
National Centre for Biomolecular Research, Faculty of Science and Central European Institute of Technology, Masaryk University, Kamenice 5, 625 00 Brno, Czech Republic

Petr Padrta, Pavel Kadeřávek:
Central European Institute of Technology, Masaryk University, Kamenice 5, 625 00 Brno, Czech Republic
pavel.kaderavek@mail.muni.cz

Milan Zachrdla, Nicolas Bolik-Coulon, Fabien Ferrage:
Laboratoire des Biomolécules, LBM, Département de chimie, École normale supérieure, PSL University, Sorbonne Université, CNRS, 75005 Paris, France
fabien.ferrage@ens.fr

Thorsten Marquardsen
Bruker BioSpin GmbH, Silberstreifen 4, 76287 Rheinstetten, Germany

Jean-Max Tyburn
Bruker BioSpin, 34 rue de l'Industrie BP 10002, 67166 Wissembourg Cedex, France

[†] authors contributed equally

Abstract

Improving our understanding of nanosecond motions in disordered proteins requires the enhanced sampling of the spectral density function obtained from relaxation at low magnetic fields. High-resolution relaxometry and two-field NMR measurements of relaxation have, so far, only been based on the recording of one- or two-dimensional spectra, which provide insufficient resolution for challenging disordered proteins. Here, we introduce a 3D-HNCO-based two-field NMR experiment for measurements of protein backbone ^{15}N amide longitudinal relaxation rates. The experiment provides accurate longitudinal relaxation rates at low field (0.33 T in our case) preserving the resolution and sensitivity typical for high-field NMR spectroscopy. Radiofrequency pulses applied on 6 different radiofrequency channels are used to manipulate the spin system at both fields. The experiment was demonstrated on the C-terminal domain of δ subunit of RNA polymerase from *Bacillus subtilis*, a protein with highly repetitive amino-acid sequence and very low dispersion of backbone chemical shifts.

Keywords: Nuclear magnetic resonance, Relaxation, Dynamics, Intrinsically disordered proteins, High-resolution relaxometry, Non-uniform sampling

1 Introduction

Nuclear magnetic resonance (NMR) is routinely used for studies of protein picosecond to nanosecond dynamics by relaxation analysis. Such relaxation studies have been successfully applied both to globular proteins and recently even to highly flexible intrinsically disordered proteins (IDPs) to describe their motion [Khan et al.(2015), Gill et al.(2016), Abyzov et al.(2016)]. Relaxation rates provide information about values of the spectral density function at discrete frequencies related to Larmor frequencies of the studied spin system. The need of high resolution and sensitivity in NMR spectroscopy of biomolecules requires the use of high magnetic fields (typically $B_0 \geq 11.74\,\mathrm{T}$). Consequently, the sampling of the spectral density functions at low frequency is limited, which leads to a lack of information about slower motions at nanosecond timescales. Access to low-frequency values of the spectral density function suitable also for biomolecular studies can be achieved by high-resolution relaxometry [Redfield(2012)]. A sample shuttle placed in the bore of a commercial high-field NMR spectrometer allows for measurements of relaxation rates over two orders of magnitude of magnetic fields (approximately in the range from 0.1–10 T). The sensitivity and resolution of high-field NMR is preserved as the detection and polarisation of the sample nuclear magnetization take place in the high-field magnetic center. The enhanced information content of relaxometry data was clearly demonstrated in studies of protein backbone motions in a structured protein [Charlier et al.(2013), Clarkson et al.(2009)] as well as, more recently, characterization of nanosecond motions in sidechains of ubiquitin [Cousin et al.(2018b)]. But, the methods reported until now provide two-dimensional spectra, which are not sufficient to study the dynamics of intrinsically disordered proteins (IDPs) with highly repetitive amino acid sequence characterized with a poor chemical shift dispersion. Another pitfall of the analysis of relaxometry relaxation rates comes from the absence of control of the spin system by radiofrequency (rf) pulses is not available once the sample leaves the high-field region equipped with an NMR probe and is moved to a low field position for relaxation. Hence, the effects of the cross-relaxation pathways cannot be suppressed by rf-pulses, relaxation decays are multi-exponential and measured relaxation rates are biased. We introduced an analysis based on simulations of the experiment [Charlier et al.(2013), Cousin et al.(2018a)] which was only verified recently, with the measurement of accurate ^{13}C relaxation rates in methyl-bearing sidechains at low field on a two-field spectrometer [Kadeřávek et al.(2019)]. Here, we introduce their counterpart developed to measure amide ^{15}N relaxation rates of proteins at low fields (0.33 T in our case). As was shown previously [Kadeřávek et al.(2019)] accurate low-field relaxation rates are essential to validate the analysis of relaxometry datasets. Accurate relaxation rates at a single low field can improve the determination of slow motions, when used in combination with conventional high-field relaxation rates. The pulse sequence is designed to overcome the limitations of currently available relaxometry experiments applied to IDPs. Previously reported high-resolution relaxometry experiments of protein backbone ^{15}N amides [Charlier et al.(2013), Clarkson et al.(2009)] are based on signal detection using

2D ^{15}N-^{1}H HSQC spectra. Here, the dimensionality of the spectra was extended with the addition of a carbonyl dimension [Srb et al.(2017)] and the evolution times in the indirect dimensions are increased using non-uniform sampling (NUS) to keep the experimental time in reasonable limits. Such an HNCO-type experiment provides a sufficient resolution for the quantitative site-specific analysis of the δ subunit of RNA polymerase with extremely low chemical shift dispersion of its intrinsically disordered and highly repetitive C-terminal domain.

2 Materials and Methods

2.1 NMR sample

The uniformly ^{13}C,^{15}N labeled sample of the δ subunit of the RNA polymerase from *Bacillus subtilis* was prepared as a recombinant protein expressed in *Escherichia coli* BL21 cells in minimal M9 media. The only source of nitrogen and carbon was ^{15}N ammonium chloride and ^{13}C glucose. The protein sample was purified as described previously [DeSaro et al.(1995)]. The NMR sample was prepared at 1.2 mM concentration in 20 mM phosphate buffer at pH 6.6 with 10 mM NaCl and 10 % D_2O. The degassed sample upon a mild vacuum was sealed in a special tube [Charlier et al.(2013)] resistant to the mechanical stress to which the sample is exposed during the sample-shuttling experiment. The design of the tube was modified to obtain an active volume of 120 μl.

2.2 NMR spectroscopy

The pulse sequence for the measurement of low-field relaxation rates is discussed in detail below. The experiment was carried out on a 600 MHz Bruker Avance-III spectrometer equipped with two TXI probes and a pneumatic shuttle system to move the sample between them [Charlier et al.(2013), Cousin et al.(2016a), Cousin et al.(2016b)]. Four 3D-HNCO spectra with different relaxation delays (20, 80, 140, and 240 ms) were acquired in an interleaved manner as a pseudo-4D experiment. The ^{15}N and ^{13}C dimensions were sampled in non-uniform sampling fashion with 688 points out of 57600 points for each of the relaxation delays. The NUS schedule was generated by an in-house program using Poisson discs sampling [Kazimierczuk et al.(2008)] with the Gauss-function used to weight the density of sampled points up to the maximum evolution times $t_{1max} = 80$ and $t_{2max} = 225$ ms for carbonyl and nitrogen dimensions, respectively. The spectral width in the indirect dimensions were 2000 and 1600 Hz for carbonyl and nitrogen dimensions, respectively. 8 scans were used to accumulate the signal. Four free induction decays were measured for each ombination of t_1 and t_2 to collect all combinations of real and imaginary components for quadrature detection in both indirect dimensions.

The design of the spectrometer allows to control the temperature at both sample positions independently. The temperature was carefully calibrated prior the measurement at both magnetic field centers to match (303.2 $\pm$ 0.2) K following the protocol for high-resolution relaxometry experiments [Cousin et al.(2018a)].

The data were processed using NMRPipe [Delaglio et al.(1995)] version 9.9 and SMILE 2.0beta [Ying et al.(2017)]. The spectra for different relaxation delays were processed inde-

pendently but the same downscaling factor was used in SMILE to prevent any uniform bias in peak intensities. No extrapolation (NUS zero-filling) was used. The spectra were analyzed using the program NMRFAM-Sparky 1.413 (T. D. Goddard and D. G. Kneller, SPARKY 3, University of California, San Francisco) [Lee et al. (2015)] and the extracted peak intensities were fitted to mono-exponential decays in the Octave 3.8.2 program [Eaton et al(2014)] (using the function *leasqr* from the package *optim*). The errors in the peak intensities were estimated from the noise in the spectra and the uncertainties of the relaxation rates were obtained from distributions of the relaxation rates generated by the smooth Bootstrap method [Tibshirani (1988), Hall(1988)] with 300 Monte Carlo simulation for each Bootstrap sample following the estimated errors in the peak intensities.

3 Results and discussion

The experiment was performed on a two-field NMR spectrometer allowing to apply rf-pulses at two different fields. The high field (14.1 T) is used for the spin polarisation during the interscan delay, recording the chemical shifts in the indirect dimensions, and for signal detection. The low-field position (0.33 T) is used for relaxation delays. The sample is moved between the two centers by a pneumatic shuttle. The scheme of the pulse sequence, based on a 3D-HNCO experiment, is shown in Figure 1. The pulse sequence starts with a refocused INEPT [Burum and Ernst(1980), Morris and Freeman(1979)] to transfer the high proton polarisation to the amide ^{15}N. ^{15}N longitudinal polarisation is used to hold the polarisation during the sample transfer to low fields due to its relatively favorable relaxation properties. The carbonyl polarisation might be at first glance even a better candidate due to the absence of strong dipole-dipole (DD) interaction with an attached proton and reduced chemical shielding anisotropy (CSA) relaxation at low fields. However, long refocused INEPT to transfer the polarisation from carbonyls to amide nitrogens at low field would result in significant losses of polarisation. In addition, inverting the carbonyl ^{13}C selectively is challenging at low field.

After the sample arrives at the low-field position proton and ^{13}C $\pi/2$ pulses are applied followed by gradients to suppress any spin orders involving protons and/or carbons, which may be built up during the sample transfer due to cross-relaxation. The same cleaning element is used before the relaxation period and again prior the sample transfer back to the high-field position. The relaxation period at low field is also preceded with a pair of INEPT steps to generate the $2N_zH_z$ two spin order and then restore back the ^{15}N polarisation. The sign of the two spin order created in the middle the two INEPT elements is alternated by a pair of phase-cycled proton $\pi/2$ pulses. This ensures that exclusively a portion of the sample inside the proton low-field coil contributes to the accumulated NMR signal (the proton coil at low field is the shortest coil in the two-field spectrometer).

A typical scheme for the relaxation delay of a longitudinal relaxation rate experiment is employed [Ferrage(2012)] with proton and carbon π pulses used to suppress the effects of dipolar cross relaxation. The application of sequences of proton and carbon π pulses with different symmetry [Levitt and Dibari(1992), Ghose(2000)] assures that the DD-DD cross-correlated cross-relaxations with the $4N_zH_zC'_z$ and $4N_zH_zC^{\alpha}_z$ three spin orders do not bias the results. On the other hand, DD-DD cross-correlated cross relaxation with $4N_zC'_zC^{\alpha}_z$ can not be suppressed at low field because it is in practice difficult to invert the carbonyl

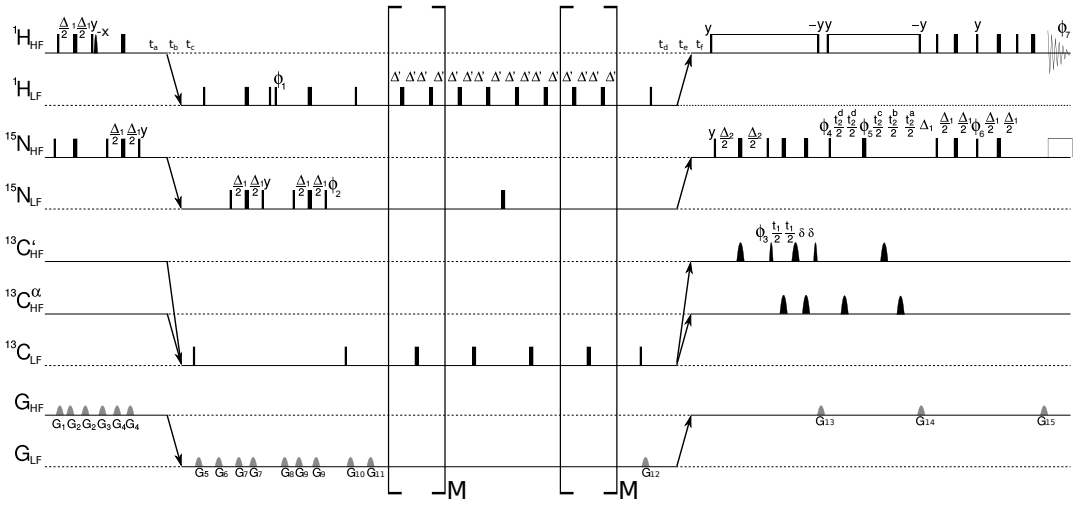

Figure 1: NMR pulse sequence for the measurement of ^{15}N longitudinal relaxation rates at 0.33 T in fully ^{13}C,^{15}N labeled proteins. The design of the two-field NMR spectrometer allows for the application of gradients, rf-pulses at two distinct magnetic fields (0.33 and 14.1 T). The gradient and rf-channels operating at high and low fields are labeled using HF and LF subscripts, respectively. Narrow and wide boxes represent hard $\pi/2$ and π pulses, respectively. The proton and ^{15}N $\pi/2$ pulse lengths at high field were 10.62 and 28.55 μs long, respectively. The duration of the low-field $\pi/2$ pulses were 10.6 μs (^{1}H), 13.3 μs (^{13}C), and 19.7 μs (^{15}N). Carbon selective pulses are used at high field to manipulate C$^{\alpha}$ carbons and carbonyls independently. The narrow semi-elliptic symbols stand for the 400 μs $\pi/2$ Q5 and Q5 time-reverse pulses [Emsley and Bodenhausen(1990)] while the wide semi-elliptic symbols stand for 256 μs long Q3 π pulses [Emsley and Bodenhausen(1990)]. The water flip-back pulse is represented by narrow semi-elliptic pulse on the proton high-field channel. The arrows represent the sample transfer between the magnetic centres by the pneumatic shuttle with durations $t_b \approx 115$ ms and $t_e \approx 155$ ms. They are flanked with pre-shuttling delays required by the instrumentation ($t_a \approx 40$ ms, $t_d \approx 30$) and stabilisation delays after the sample transfer ($t_c = 20$ ms, $t_f = 50$ ms). Various relaxation delays were achieved by different number of repetitions M of the segments in the brackets. The constant and the initial delays used in the pulse program follows: Δ' = 2.5 ms, $\Delta_1 = 1/(4J_{NH})$, $\Delta_2 = 1/(4_{NC'})$, t_2^a= 0.75 ms, $t_2^b = t_2^d = 6.25$ ms, $t_2^c = 0$. Decoupling pulse trains are depicted as open wide boxes (GARP [Shaka et al.(1985)] is used for ^{15}N during the signal acquisition, and WALTZ65 [Shaka et al.(1983)] for proton decoupling). All pulses are applied along the x axis of the rotating frame, unless indicated otherwise: ϕ_1 = y,y,-y-y, ϕ_2 = 4y, 4(-y), ϕ_3 = x, ϕ_4 = x, ϕ_5 = x,y,-x, -y, ϕ_6 = -y , ϕ_7 = x,-x,-x,x,-x,x,x-x. Sine-shaped gradients with duration 0.9 ms were applied along z-direction with the following amplitudes: G_1 = 5.75 G/cm, G_2 = 0.75 G/cm, G_3 = 7.75 G/cm, G_4 = 0.6 G/cm, G_5 = 8.5 G/cm, G_6 = 5.5 G/cm G_7 = 3.5 G/cm, G_8 = 9.5 G/cm, G_9 = -7.5 G/cm, G_{10} = 11.5 G/cm, G_{11} = 16.5 G/cm, G_{12} = -4.5 G/cm, G_{13} = 9.25 G/cm, G_{14} = 20 G/cm, G_{15} = 2.025 G/cm. Quadrature detection was achieved with States [States et al.(1982)] and Echo-AntiEcho [Palmer et al.(1991)](with the alternation sign of gradient G_{14}) methods in carbonyl and amide indirect dimensions, respectively.

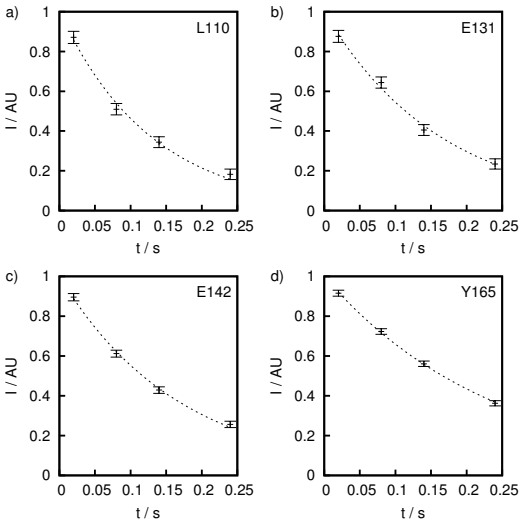

Figure 2: Longitudinal relaxation decays (normalized so that the pre-exponential factor is unity) fitted with mono exponential decays (dotted lines) for residues L110 (a), E131 (b), E142 (c), and Y165 (d) of δ subunit of RNA polymerase from *Bacillus subtilis*.

and C^{α} polarisation selectively (120 ppm difference between them corresponds only to 422 Hz requiring a very long selective pulse). However, it can be shown that the discussed cross-relaxation rate has virtually no effect on the measured ^{15}N amide longitudinal auto-relaxation rate. A simulation showed that the ^{15}N longitudinal relaxation rate is at least 500 times larger than the DD-DD cross-correlated cross relaxation rate towards $4N_zC'_zC^{\alpha}_z$ for magnetic fields ranging from 0.1 to 20 T and correlation time of motion between 1 ps and 100 ns.

After the transfer back to high field the labeling of carbonyl and amide nitrogen chemical shifts is performed using a semi-constant time incrementation for the ^{15}N dimension [Grzesiek and Bax(1990)]. Finally, the signal is transferred to the amide proton for detection. The acquisition of the full 3D HNCO type experiment would require more than 50 days with the desired resolution and selected experimental setup. Therefore, a non-uniform sampling method has been used to reduce the experimental time (see Materials and Methods section).

The experiment was performed with a sample of the δ subunit of RNA polymerase from *Bacillus subtilis* which makes transcription sensitive to regulation by the concentration of the initiating nucleotide triphosphates [Rabatinová et al.(2013)]. The δ subunit consists of a structured N-terminal domain [Motáčková et al.(2010)] and a disordered C-terminal domain. The high abundance of aspartic and glutamic acids in the C-terminal domain makes it mostly negatively charged, except for a lysine stretch (residues 96-104). Transient contacts between the positively charged lysine stretch and remaining parts of the molecule are important for the δ subunit function and were investigated in previous studies [Papoušková et al.(2013), Kubáň et al.(2019)].

Examples of peak intensity decays are shown in Figure 2 and supplementary information material Figures S1–S3. Longitudinal relaxation rates measured at 0.33 T are shown in

Figure 3 together with the previously reported [Srb et al.(2017)] longitudinal and transverse relaxation rates acquired at 14.1 T for the same system under the same conditions. All discussed experiments were performed with uniformly ^{13}C, ^{15}N labeled samples, so the auto-relaxation rates reflect not only the relaxation due to the direct ^{1}H-^{15}N DD interaction together with the contribution of the anisotropy of the amide ^{15}N chemical shielding tensor (CSA), but also the effects of the dipolar interactions between the ^{15}N and neighboring ^{13}C nuclei as discussed previously [Srb et al.(2017)]. Although 48 out of 68 residues in the negatively charged part of the C-terminal domain are either glutamic or aspartic acids in this part of the sequence, resulting in very poor signal dispersion, we were able to extract quantitative information for 80% of them. The relaxation delays were chosen to cover primarly slower relaxation rates. Therefore, the values for the rapidly relaxing lysine stretch were obtained with lower precisions and are not presented.

The quantitative analysis of NUS spectra is known to be possible [Mayzel et al. (2017)] if somewhat challenging [Mobli and Hoch (2014), Shchukina et al.(2018), Stetz and Wand(2016)]. In order to verify the extracted quantitative information we compared processing with the SMILE package [Ying et al.(2017)] with other softwares: SCRUB [Coggins et al.(2012)] and MDD [Orekhov and Jaravine (2011), Linnet and Teilum (2016)] using coprocessing with additional spectra measured with the same setup of the spectral resolutions and spectral widths (supplementary information material Figure S4). Seven residues (109, 117, 121, 124, 154, 158, and 166) were excluded from the analysis to guarantee a high reliability of the presented results.

Unlike the relatively flat profile of longitudinal relaxation rates acquired at 14.1 T, the data reported here show significantly more variations over the protein sequence because they are more sensitive to slower motions. The largest relaxation rates were measured for the segment of residues 114–122 forming transient contacts with the positively charged lysine stretch. Locally larger relaxation rates were measured for residues 141-144 and around the residue 155.

Similar features and trends can be found also in the profile of the transverse relaxation rates which are dependent on the values of the spectral density function at the zero frequency. In contrast to transverse relaxation rates, the longitudinal relaxation rates at low field can not be biased by contributions of a chemical exchange. High-field transverse cross-correlated cross-relaxation rates (CSA-DD) is another relaxation rate which is not sensitive to contributions of chemical exchange [Abyzov et al.(2016), Khan et al.(2015), Srb et al.(2017), Kadeřávek et al.(2014)]. However, unless the analysis is based on both longitudinal and transverse CSA/DD cross-correlated cross relaxation [Kroenke et al.(1998)], the analysis combining the auto-relaxation rates and transverse CSA-DD cross-correlated cross-relaxation rates requires a very accurate determination of amplitudes and orientations of amide chemical shielding tensors which may also vary over the sequence of proteins and might be difficult to obtain. In contrast to that approach, the data obtained in the presented experiment are insensitive to the chemical shielding anisotropy (CSA). A simulation shows that the contribution of the CSA relaxation mechanism to the ^{15}N longitudinal auto-relaxation rate at 0.33 T is below 0.11% for proteins with correlation times up to 100 ns.

Measuring longitudinal relaxation rates at 0.33 T gives access to values of the spectral density functions at low frequencies. This provides unique information, sampling the spectral density function where it varies due to nanosecond motions. The slowest motions for which the inflection point is reached are defined by the ^{15}N Larmor frequency ω_N. At 14.1 T (^{15}N

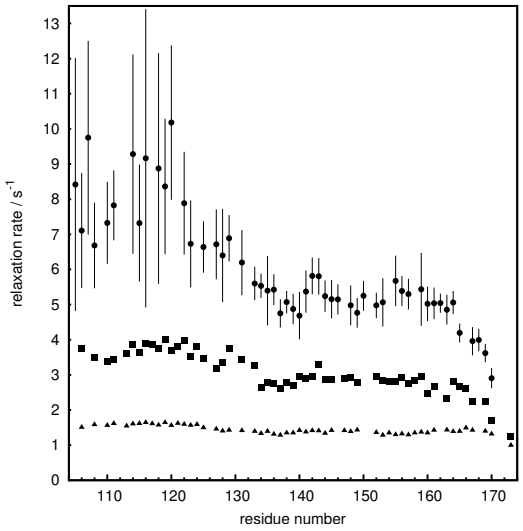

Figure 3: Longitudinal relaxation rates at 0.33 T measured with the two-field NMR spectrometer (circles) compared to previously reported values of transverse (squares) and longitudinal relaxation rates (triangles) measured at 14.1 T. Data were measured on an uniformly ^{13}C, ^{15}N labeled samples of the δ subunit of RNA polymerase from *Bacillus subtilis*. Only data corresponding to the disordered C-terminal domain is displayed. The standard deviations of the data measured at 14.1 T are lower than $0.1\,\mathrm{s}^{-1}$ and are not displayed as error-bars.

frequency −60.85 MHz) the limiting correlation time (given by the inflection point of the spectral density function $\tau = 1/(\omega_N\sqrt{3})$) is $\tau \approx 1.5$ ns compared to correlation times as long as $\tau \approx 64.5$ ns probed at 0.33 T (^{15}N frequency −1.42 MHz) which is valuable for systems where the correlation function has still non-zero values for times longer than 65 ns, allowing to study very slow motions.

4 Conclusion

A new pulse sequence for the measurement of accurate longitudinal relaxation rates at a low magnetic field with a two-field NMR spectrometer is presented. This pulse sequence may also be used for high-resolution relaxometry, simply omitting the pulses at low field. The pulse sequence is designed to be suitable for the analysis of the dynamics of IDPs as was shown for the C-terminal domain of the δ subunit of RNA polymerase - a protein with highly repetitive amino acid sequence and characterized by very low diversity of NMR frequencies of backbone nuclei. Relaxation rates measured at low field identify segments with slower motional modes within the disordered region of the δ subunit in agreement with previous studies [Srb et al.(2017), Kadeřávek et al.(2014)].

We demonstrated that the presented two-field NMR experiment can be used for the measurements of backbone amide ^{15}N longitudinal relaxation rates at very low fields. Such unique information will be useful for studies of protein backbone motions.

5 acknowledgements

This work was supported by Czech Science Foundation grant No. GA18-04197Y and grant No. ANR-18-CE29-0003 provided by agence nationale de la recherche. Short scientific mission of PK to perform measurements at the two-field NMR spectrometer was supported by STSM Grant from the EURELAX COST Action CA15209.

Conflict of interest

Thorsten Marquardsen and Jean-Max Tyburn are employees of the Bruker BioSpin. The authors declare no other conflict of interest.

References

[Abyzov et al.(2016)] Abyzov A, Salvi N, Schneider R, Maurin D, Ruigrok RWH, Jensen MR, Blackledge M (2016) Identification of Dynamic Modes in an Intrinsically Disordered Protein Using Temperature-Dependent NMR Relaxation. J Am Chem Soc 138(19):6240–6251

[Burum and Ernst(1980)] Burum D, Ernst R (1980) Net polarization transfer via a J-ordered state for signal enhancement of low-sensitivity nuclei. J Magn Reson 39(1):163–168

[Charlier et al.(2013)] Charlier C, Khan SN, Marquardsen T, Pelupessy P, Reiss V, Sakellariou D, Bodenhausen G, Engelke F, Ferrage F (2013) Nanosecond Time Scale Motions in Proteins Revealed by High-Resolution NMR Relaxometry. J Am Chem Soc 135(49):18665–18672

[Clarkson et al.(2009)] Clarkson MW, Lei M, Eisenmesser EZ, Labeikovsky W, Redfield A, Kern D (2009) Mesodynamics in the SARS nucleocapsid measured by NMR field cycling. J Biomol NMR 45(1–2):217-225

[Coggins et al.(2012)] Coggins BE, Werner-Allen JW, Yan A, Zhou P (2012) Rapid protein global fold determination using ultrasparse sampling, high-dynamic range artifact suppression, and time-shared NOESY. J Am Chem Soc 134(45):18619–18630

[Cousin et al.(2016a)] Cousin SF, Charlier C, Kadeřávek P, Marquardsen T, Tyburn JM, Bovier PA, Ulzega S, Speck T, Wilhelm D, Engelke F, Maas W, Sakellariou D, Bodenhausen G, Pelupessy P, Ferrage F (2016a) High-resolution two-field nuclear magnetic resonance spectroscopy. Phys Chem Chem Phys 18(48):33187–33194

[Cousin et al.(2016b)] Cousin SF, Kadeřávek P, Haddou B, Charlier C, Marquardsen T, Tyburn JM, Bovier PA, Engelke F, Maas W, Bodenhausen G, Pelupessy P, Ferrage F (2016b) Recovering Invisible Signals by Two-Field NMR Spectroscopy. Angew Chem-Int Edit 55(34):9886–9889

[Cousin et al.(2018a)] Cousin SF, Kadeřávek P, Bolik-Coulon N, Ferrage F (2018) Determination of Protein ps-ns Motions by High-Resolution Relaxometry. Methods Mol Biol 1688:169–203

[Cousin et al.(2018b)] Cousin SF, Kadeřávek P, Bolik-Coulon N, Gu Y, Charlier C, Garber L, Bruschweiler-Li L, Marquardsen T, Tyburn JM, Bruschweiler R, Ferrage F (2018) Time-Resolved Protein Side-Chain Motions Unraveled by High-Resolution Relaxometry and Molecular Dynamics Simulations. J Am Chem Soc 140(41):13456–13465

[Delaglio et al.(1995)] Delaglio F, Grzesiek S, Vuister G, Zhu G, Pfeifer J, Bax A (1995) NMRPipe - A multidimensional spectral processing system based on UNIX pipes. J Biomol NMR 6:277–293

[DeSaro et al.(1995)] DeSaro F, Woody A, Helmann J (1995) Structural-analysis of the *Bacillus-subtilis* delta-factor - a protein polyanion which displaces RNA from RNA-polymerase. J Mol Biol 252(2):189–202

[Eaton et al(2014)] Eaton JW, Bateman D, Hauberg S, and Wehbring R (2014) GNU Octave version 3.8.1 manual: a high-level interactive language for numerical computations. CreateSpace Independent Publishing Platform, http://www.gnu.org/software/octave/doc/interpreter

[Emsley and Bodenhausen(1990)] Emsley L, Bodenhausen G (1990) Gaussian pulse cascades - new analytical functions for rectangular selective inversion and in-phase excitation in NMR. Chem Phys Lett 165(6):469–476

[Ferrage(2012)] Ferrage F (2012) Protein Dynamics by ^{15}N Nuclear Magnetic Relaxation. Methods Mol Biol 831:141–163

[Ghose(2000)] Ghose R (2000) Average Liouvillian theory in nuclear magnetic resonance - Principles, properties, and applications. Concepts Magn Reson 12(3):152–172

[Gill et al.(2016)] Gil Ml, Byrd RA, Palmer AG (2016)Dynamics of GCN4 facilitate DNA interaction: a model-free analysis of an intrinsically disordered region. Phys Chem Chem Phys 18(8):5839-5849

[Grzesiek and Bax(1990)] Grzesiek S, Bax A (1993) Amino acid type determination in the sequential assignment procedure of uniformly 13C/15N-enriched proteins. J Biomol NMR 3:185–204

[Hall(1988)] Hall, P. (1988) Theoretical comparison of bootstrap confidence intervals. Ann Statisi 16:1–50

[Kadeřávek et al.(2019)] Kadeřávek P, Bolik-Coulon N, Cousin SF, Marquardsen T, Tyburn JM, Dumez JN, Ferrage F (2019) Protein Dynamics from Accurate Low-Field Site-Specific Longitudinal and Transverse Nuclear Spin Relaxation. J Phys Chem Lett 101(19):5917–5922

[Kadeřávek et al.(2014)] Kadeřávek P, Zapletal V, Rabatinová A, Krasný L, Sklenář V, Žídek L (2014) Spectral density mapping protocols for analysis of molecular motions in disordered proteins. J Biomol NMR 58(3):193–207

[Kazimierczuk et al.(2008)] Kazimierczuk K, Zawadzka A, Kozminski W (2008) Optimization of random time domain sampling in multidimensional NMR. J Magn Reson 192(1):123–130

[Khan et al.(2015)] Khan SN, Charlier C, Augustyniak R, Salvi N, Dejean V, Bodenhausen G, Lequin O, Pelupessy P, Ferrage F (2015) Distribution of Pico- and Nanosecond Motions in Disordered Proteins from Nuclear Spin Relaxation. Biophys J 109(5):988–999

[Kroenke et al.(1998)] Kroenke CD, Loria JP, Lee LK, Rance M, Palmer AG (1998) Longitudinal and transverse ^{1}H-^{15}N dipolar ^{15}N chemical shift anisotropy relaxation interference: Unambiguous determination of rotational diffusion tensors and chemical exchange effects in biological macromolecules. J Am Chem Soc 120(31):7905–7915

[Kubáň et al.(2019)] Kubáň V, Srb P, Stegnerová H, Padrta P, Zachrdla M, Jaseňáková Z, Šanderová H, Vítovská D, Krásný L, Koval T, Dohnálek J, Ziemska-Legicka J, Grynberg M, Jarnot P, Gruca A, Jensen MR, Blackledge M, Žídek L (2019) Quantitative Conformational Analysis of Functionally Important Electrostatic Interactions in the Intrinsically Disordered Region of Delta Subunit of Bacterial RNA Polymerase. J Am Chem Soc accepted

[Lee et al. (2015)] Lee W, Tonelli M, Markley JL (2015) NMRFAM-SPARKY: enhanced software for biomolecular NMR spectroscopy. Bioinformatics 31(8):1325–1327

[Levitt and Dibari(1992)] Levitt MH, Dibari L (1992)Steady-state in magnetic-resonance pulse experiments. Phys Rev Lett 69(21):3124–3127

[Linnet and Teilum (2016)] Linnet TE, Teilum K (2016)Non-uniform sampling of NMR relaxation data. J Biomol NMR 64:165–173

[Mayzel et al. (2017)] Mayzel M, Ahlner A, Lundström P, Orekhov VY (2017) Measurement of protein backbone (CO)-C-13 and N-15 relaxation dispersion at high resolution. J Biomol NMR 69(1):1–12

[Mobli and Hoch (2014)] Mobli M, Hoch JC (2014) Nonuniform sampling and non-Fourier signal processing methods in multidimensional NMR. Prog Nucl Magn Res Spectrosc. 83:21–41

[Morris and Freeman(1979)] Morris G, Freeman R (1979) Enhancement of nuclear magnetic-resonance signals by polarization transfer. J Am Chem Soc 101(3):760–762

[Motáčková et al.(2010)] Motáčková V, Šanderová H, Žídek L, Nováček J, Padrta P, Švenková A, Korelusová J, Jonák J, Krásný L, Sklenářr V. (2010) Solution structure of the Nterminal domain of Bacillus subtilis δ subunit of RNA polymerase and its classification based on structural homologs. Proteins 78(7):1807–1810

[Orekhov and Jaravine (2011)] Orekhov VY, Jaravine VA (2011) Analysis of non-uniformly sampled spectra with multi-dimensional decomposition. Prog Nucl Magn Res Spectrosc. 59(3):271–292

[Palmer et al.(1991)] Palmer A, Cavanagh J, Wright P, Rance M (1991) Sensitivity improvement in proton-detected 2-dimensional heteronuclear correlation NMR-spectroscopy. J Magn Reson 93(1):151–170

[Papoušková et al.(2013)] Papoušková V, Kadeřávek P, Otrusinová O, Šanderová H, Nováček J, Krásný L, Sklenář V, Žídek L (2013) Structural Study of the Partially Disordered Full-Length delta Subunit of RNA Polymerase from Bacillus subtilis. ChemBioChem 14(14):1772–1779

[Rabatinová et al.(2013)] Rabatinová A, Matějíčková JJ, Korelusová J, Sojka L, Papoušková V, Sklenář V, Žídek L Krásný L (2013) The delta Subunit of RNA Polymerase Is Required for Rapid Changes in Gene Expression and Competitive Fitness of the Cell. J Bacteriol 195(11):2603–2611

[Redfield(2012)] Redfield AG (2012) High-resolution NMR field-cycling device for full-range relaxation and structural studies of biopolymers on a shared commercial instrument. J Biomol NMR 52(2):159–177

[Shaka et al.(1983)] Shaka A, Keeler J, Frenkiel T, Freeman R (1983) An improved sequence for broad-band decoupling - WALTZ-16. J Magn Reson 52(2):335–338

[Shaka et al.(1985)] Shaka A, Barker P, Freeman R (1985) Computer-optimized decoupling scheme for wideband applications and low-level operation. J Magn Reson 64(3):547–552

[Shchukina et al.(2018)] Shchukina A, Urbańnczyk M, Kasprzak P, Kazimierczuk K (2018) Alternative data processing techniques for serial NMRexperiments. Concepts Magn Reson Part A. 46A:e21429:1–11

[Srb et al.(2017)] Srb P, Nováček J, Kadeřávek P, Rabatinová A, Krásný L, Žídková J, Bobalová J, Sklenář V, Žídek L (2017) Triple resonance NMR relaxation experiments for studies of intrinsically disordered proteins. J Biomol NMR 69(3):133–146

[States et al.(1982)] States DJ, Haberkorn RA, Ruben DJ (1982) A Two-Dimensional Nuclear Overhauser Experiment with Pure Absorption Phase in Four Quadrants. J Magn Reson 48(2):286–292

[Stetz and Wand(2016)] Stetz MA, Wand AJ (2016) Accurate determination of rates from non-uniformly sampled relaxation data. J Biomol NMR 65(3–4):157–170

[Tibshirani (1988)] Tibshirani R (1988) Variance stabilization and the bootstrap. Biometrika 75(3):433–444

[Ying et al.(2017)] Ying J, Delaglio F, Torchia DA, Bax A (2017) Sparse multidimensional iterative lineshape-enhanced (SMILE) reconstruction of both non-uniformly sampled and conventional NMR data. J Biomol NMR 68(2, SI):101–118

Supplementary information to: J Biomol NMR

Boosting the resolution of low-field ^{15}N relaxation experiments on intrinsically disordered proteins with triple-resonance NMR

Zuzana Jaseňáková†, Vojtěch Zapletal†, Petr Padrta†, Milan Zachrdla, Nicolas Bolik-Coulon, Thorsten Marquardsen, Jean-Max Tyburn, Lukáš Žídek, Fabien Ferrage*, Pavel Kadeřávek*

Zuzana Jaseňáková · Vojtěch Zapletal · Lukáš Žídek
National Centre for Biomolecular Research, Faculty of Science and Central European Institute of Technology, Masaryk University, Kamenice 5, 625 00 Brno, Czech Republic
Central European Institute of Technology, Masaryk University, Kamenice 5, 625 00 Brno, Czech Republic

Petr Padrta · Pavel Kadeřávek
Central European Institute of Technology, Masaryk University, Kamenice 5, 625 00 Brno, Czech Republic
e-mail: pavel.kaderavek@mail.muni.cz

Milan Zachrdla · Nicolas Bolik-Coulon · Fabien Ferrage
Laboratoire des Biomolécules, LBM, Département de chimie, École normale supérieure, PSL University, Sorbonne Université, CNRS, 75005 Paris, France
e-mail: fabien.ferrage@ens.fr

Thorsten Marquardsen
Bruker BioSpin GmbH, Silberstreifen 4, 76287 Rheinstetten, Germany

Jean-Max Tyburn
Bruker BioSpin, 34 rue de l'Industrie BP 10002, 67166 Wissembourg Cedex, France

† authors contributed equally

Table S1: The fitted longitudinal relaxation rates measured at 0.33 T of the C-terminal domain of δ subunit of RNA polymerase from *Bacillus subtilis* together with the mean (third column) and standard deviation (fourth column) of the distribution obtained by the smooth Bootstrap method.

residue number	fitted R_1/s^{-1}	mean R_1/s^{-1}	R_1 standard deviation $/\mathrm{s}^{-1}$
105	9.3	8.4	3.6
106	7.0	7.1	1.6
107	9.9	9.7	2.8
108	6.7	6.7	1.2
110	7.7	7.3	1.2
111	7.7	7.8	1.0
114	8.8	9.3	2.8
115	8.0	7.3	1.7
116	8.6	9.2	4.2
118	7.8	8.9	3.3
119	8.9	8.4	1.9
120	11.2	10.2	2.2
122	8.1	7.9	1.5
123	7.0	6.7	1.2
125	6.5	6.6	0.7
127	6.6	6.7	1.0
128	6.9	6.4	1.3
129	6.9	6.9	0.7
131	6.1	6.2	0.9
133	5.5	5.6	0.5
134	5.6	5.5	0.3
135	5.2	5.4	1.0
136	5.4	5.4	0.4
137	4.8	4.8	0.4
138	5.0	5.1	0.3
139	4.9	4.9	0.4
140	4.8	4.7	0.7
141	5.4	5.4	0.6
142	5.9	5.8	0.5
143	5.8	5.8	0.5
144	5.3	5.2	0.4
145	5.3	5.2	0.5
146	5.1	5.1	0.4
148	4.9	5.0	0.6
149	4.7	4.8	0.4
150	5.3	5.2	0.4
152	5.0	5.0	0.4
153	5.1	5.1	0.7

Continued on next page

Table 1 – *Continued from previous page*

residue number	fitted R_1/s^{-1}	mean R_1/s^{-1}	R_1 standard deviation $/\mathrm{s}^{-1}$
155	5.8	5.7	0.7
156	5.3	5.4	0.4
157	5.2	5.3	0.4
159	5.7	5.4	1.0
160	5.0	5.0	0.5
161	5.1	5.0	0.4
162	5.0	5.0	0.3
163	4.9	4.9	0.4
164	5.1	5.1	0.3
165	4.2	4.2	0.3
167	4.0	4.0	0.4
168	4.0	4.0	0.3
169	3.6	3.6	0.3
170	2.9	2.9	0.3

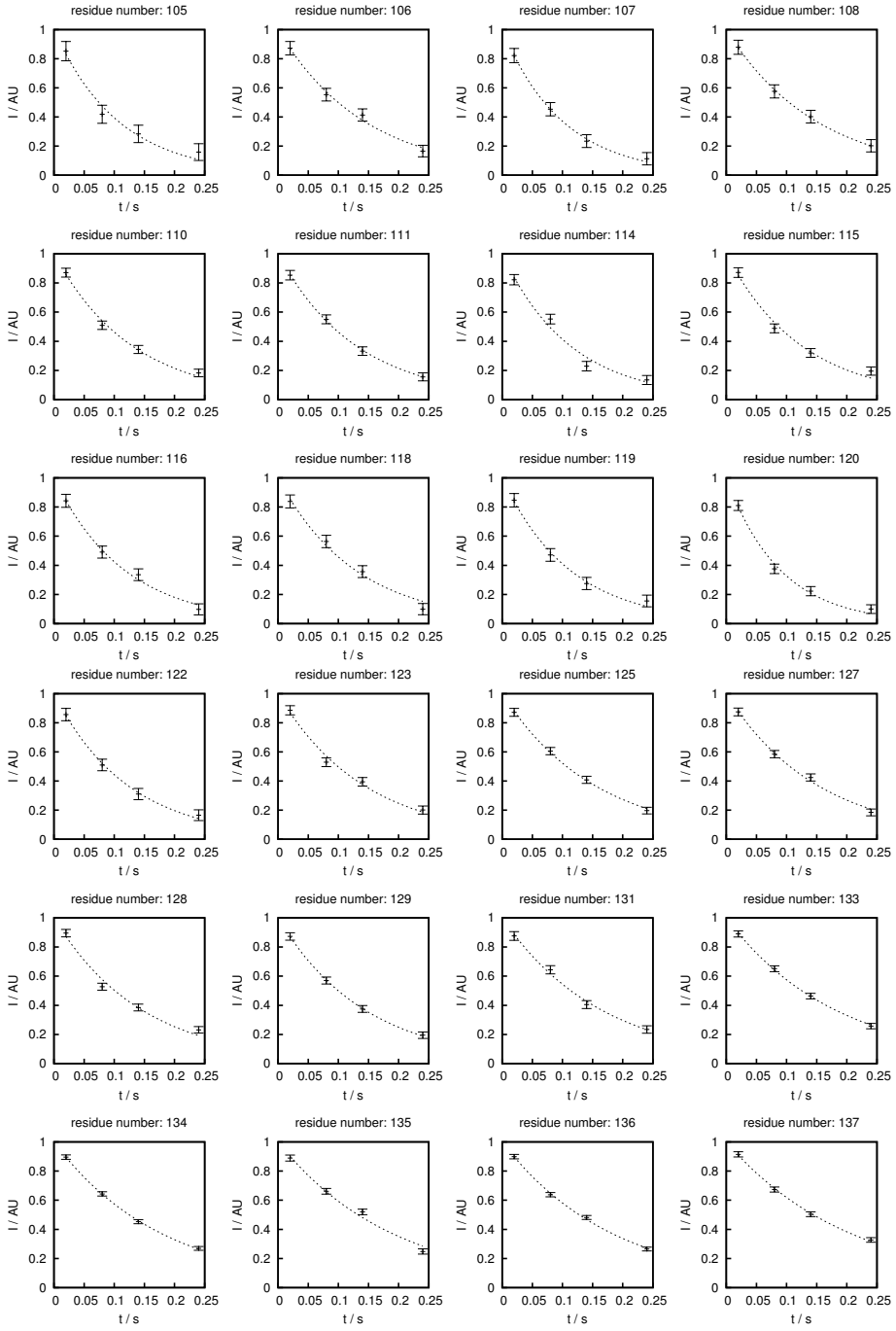

Figure S1: Experimental longitudinal relaxation decays (normalized so that the pre-exponential factor is unity) and the fitted mono exponential decays (dotted lines) for residues 105–134 of the δ subunit of RNA polymerase from *Bacillus subtilis*.

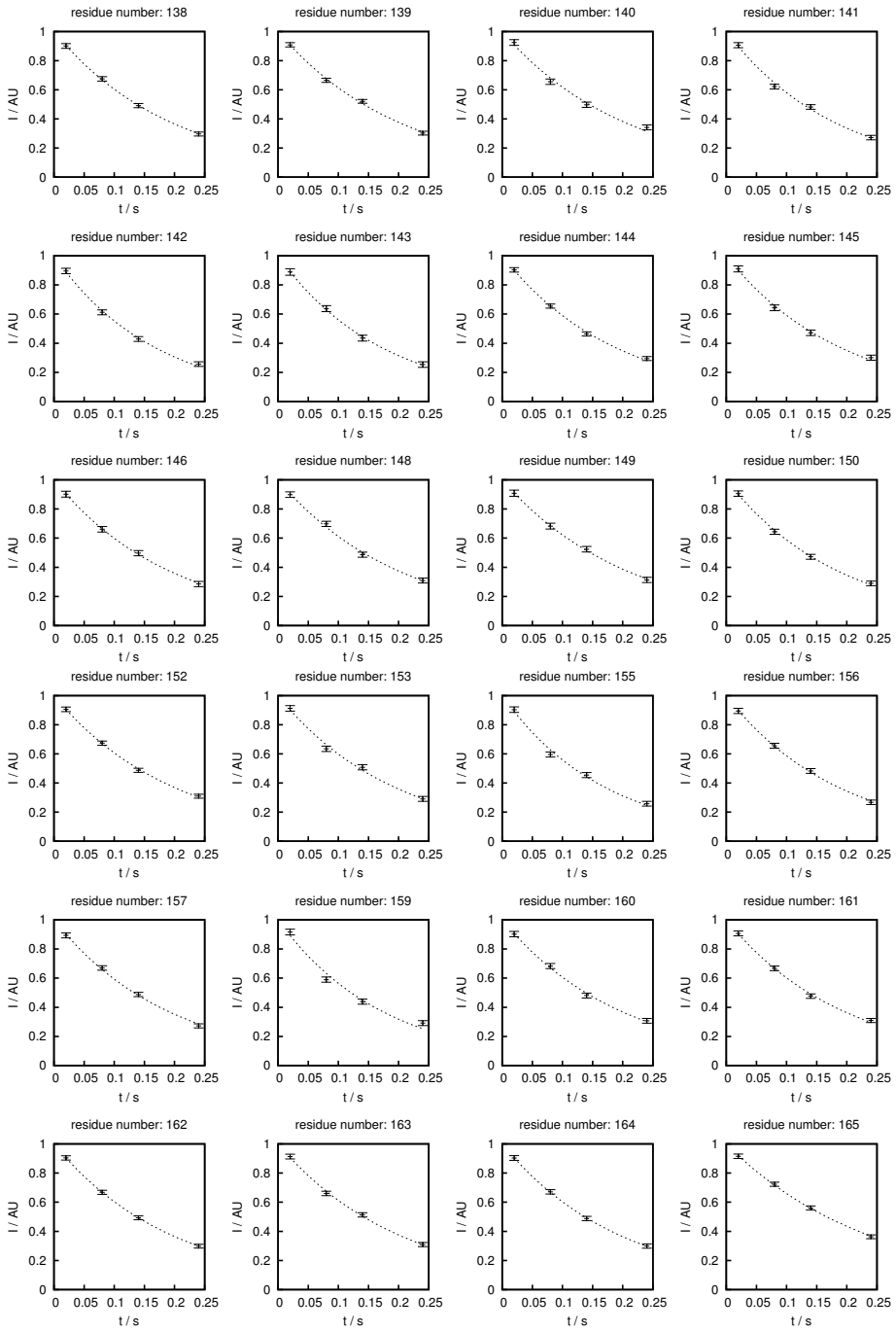

Figure S2: Experimental longitudinal relaxation decays (normalized so that the pre-exponential factor is unity) and the fitted mono exponential decays (dotted lines) for residues 135–162 of the δ subunit of RNA polymerase from *Bacillus subtilis*.

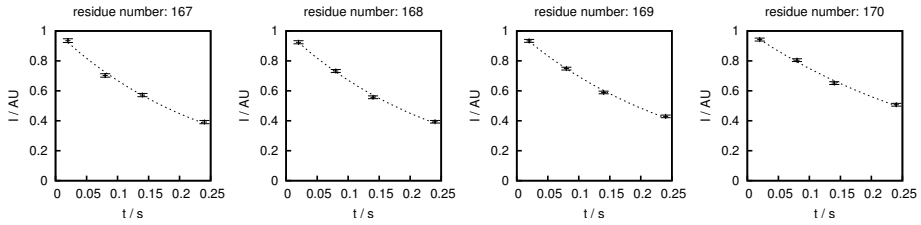

Figure S3: Experimental longitudinal relaxation decays (normalized so that the pre-exponential factor is unity) and the fitted mono exponential decays (dotted lines) for residues 163–170 of the δ subunit of RNA polymerase from *Bacillus subtilis*.

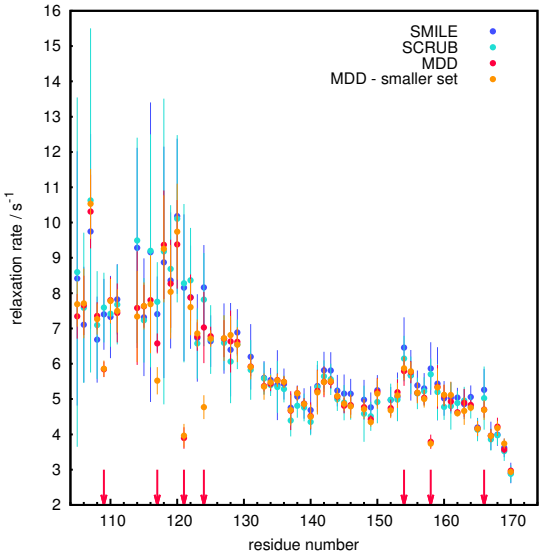

Figure S4: Comparison of the relaxation rates obtained by different processing methods: SMILE [Ying et al.(2017)] (blue), SCRUB [Coggins et al.(2012)] (cyan), MDD[Orekhov and Jaravine (2011), Linnet and Teilum (2016)] (red), and MDD with fewer NUS points (orange). MDD processing of the measured spectra was performed with additional spectra (measured with identical spectral widths and resolutions) to enable coprocessing effect. Orange points represent results of the same MDD coprocessing as results shown in red, but the number of NUS points was reduced to test the robustness of the processing. Red arrows highlight the residues which were excluded from the analysis to guarantee a high reliability of the presented results.

References

[Coggins et al.(2012)] Coggins BE, Werner-Allen JW, Yan A, Zhou P (2012) Rapid protein global fold determination using ultrasparse sampling, high-dynamic range artifact suppression, and time-shared NOESY. J Am Chem Soc 134(45):18619–18630

[Linnet and Teilum (2016)] Linnet TE, Teilum K (2016)Non-uniform sampling of NMR relaxation data. J Biomol NMR 64:165–173

[Orekhov and Jaravine (2011)] Orekhov VY, Jaravine VA (2011) Analysis of non-uniformly sampled spectra with multi-dimensional decomposition. Prog Nucl Magn Res Spectrosc. 59(3):271–292

[Ying et al.(2017)] Ying J, Delaglio F, Torchia DA, Bax A (2017) Sparse multidimensional iterative lineshape-enhanced (SMILE) reconstruction of both non-uniformly sampled and conventional NMR data. J Biomol NMR 68(2, SI):101–118